Carbon 96 (2016) 139–144

Contents lists available at ScienceDirect

Carbon

journal homepage: www.elsevier.com/locate/carbon

Facile synthesis of carbon dot-Au nanoraspberries and their application as high-performance counter electrodes in quantum dot-sensitized solar cells

Van-Duong Dao [a], Poeun Kim [b, e], Seunghyeon Baek [c], Liudmila L. Larina [a, d], Kijung Yong [c], Ryong Ryoo [b, e], Seung Hyeon Ko [e, **], Ho-Suk Choi [a, *]

[a] Department of Chemical Engineering, Chungnam National University, 220 Gung-Dong, Yuseong-Gu, Daejeon 305-764, Republic of Korea
[b] Department of Chemistry, Korea Advanced Institute of Science and Technology (KAIST), Daejeon 305-701, Republic of Korea
[c] Department of Chemical Engineering, Pohang University of Science and Technology (POSTECH), Pohang 790-784, Republic of Korea
[d] Department of Solar Photovoltaics, Institute of Biochemical Physics of Russian Academy of Sciences, Russia
[e] Center for Nanomaterials and Chemical Reactions, Institute for Basic Science (IBS), Yuseong-Gu, Daejeon 305-701, Republic of Korea

ARTICLE INFO

Article history:
Received 19 June 2015
Received in revised form
19 August 2015
Accepted 5 September 2015
Available online 8 September 2015

ABSTRACT

Carbon dot-Au nanoraspberries (Cdot-Au NRs) were synthesized by a simple one-pot process using Cdots as initiators to direct the dendritic growth of Au via room temperature chemical reduction of $HAuCl_4$ by formic acid. We evaluated the resulting Cdot-Au NR as a counter electrode material for ZnO nanowire/CdS/CdSe quantum dot-sensitized solar cells (QDSCs). The counter electrode employing Cdot-Au NRs exhibited higher electrocatalytic activity, lower charger-transfer resistance, and larger exchange current density than commonly used Au-sputtered counter electrodes. The power conversion efficiency of the cell was improved to 5.4%, in comparison to efficiencies of 3.6% and 0.18% shown by cells employing Au-sputtered and Cdot counter electrodes, respectively. These features render Cdot-Au NRs as highly promising counter electrode materials for QDSCs.

1. Introduction

Quantum dot-sensitized solar cells (QDSCs) have attracted immense interest as promising next-generation photovoltaic (PV) systems [1] because of the unique properties of quantum dots (QDs), such as high extinction coefficients, broad spectral ranges, and easily tunable band gaps [2]. The challenges involved in realizing the full potential of QDSCs include improving the energy conversion efficiency and reducing costs. To achieve higher conversion efficiencies, a variety of QD sensitizers have been widely explored [3–6]. A highest efficiency of 8.5% has been reported with Sb_2S_3 and PbS QDs at the laboratory scale [4].

The counter electrode (CE) is an important component in solar cells and considerable efforts have been directed toward finding appropriate materials to fabricate CEs with lower resistances and higher reduction rates of the redox electrolyte. Pt CEs have been widely used as the standard CE; however, due to the adsorption of sulfides on its surface, the use of Pt as the CE limits the QDSC performance [7–9]. Au CEs have been considered as alternatives because of their high chemical stability against sulfide ions. However, since cost reduction is a critical factor in the development of solar cells, various materials have been extensively explored as an inexpensive alternative for Au CE, including transition metal sulfides [10–13], carbonaceous materials [1,14–18], and conductive polymers [19,20]. Among these, carbon-coated CEs have been widely tested to optimize the cell performance using several types of carbon materials. In the case of CEs using graphene, the defective sites on graphene provides the active sites for catalyzing the triiodide reduction in dye-sensitized solar cells (DSCs) [21]. As a proof of concept, carbon dot (Cdot)-doped polypyrrole [22] was evaluated as a CE material in DSCs. The results show that the edge-bound nanoscale Cdots provide more electrochemically active sites and a higher charge transfer rate because of the presence of a higher number of active defect sites on the Cdot surface. Furthermore, the doping of Cdots led to a more porous CE, resulting in an increased number of electrocatalytic active centers and enhancement of the reactant diffusion.

* Corresponding author.
** Corresponding author.
E-mail addresses: shsarahko@gmail.com (S.H. Ko), hchoi@cnu.ac.kr (H.-S. Choi).

http://dx.doi.org/10.1016/j.carbon.2015.09.023
0008-6223/

On the other hand, the material structure and morphology of the CE affect the catalytic activity and performance of the solar cell by providing a different active catalytic surface (i.e., surface area, number of active sites, etc.) for the redox reactions [22–24]. For instance, Chen et al. compared previously reported energy conversion efficiencies of QDSCs using various CEs coated with copper sulfide of different morphologies and have shown that the efficiency typically ranges from 3.73 to 5.21% [24]. The efficiencies are low, indicating that the polysulfide electrolyte diffusion and the surface active sites are to be further improved.

Here, we report a facile one-pot method to synthesize Cdot-Au nanoraspberries (NRs) consisting of a dense array of Au branches. In this approach, Cdots with an average size of 1.2 nm were used as initiators to induce the anisotropic growth of Au via a simple room temperature chemical reduction of $HAuCl_4$ by formic acid. Using this synthesis, we reproducibly prepared Cdot-Au NRs with high surface areas. High-angle annular dark field scanning transmission electron microscopy (HAADF-STEM) and energy dispersive spectroscopy (EDS) elemental mapping revealed that the resulting Cdot-Au NR composite material exhibits homogeneous distribution of carbon and Au throughout the raspberry-like structure. These Cdot-Au NRs displayed an enhanced catalytic activity toward polysulfide electrolyte reduction as a CE in ZnO nanowire/CdS/CdSe QDSCs, which increased the power conversion efficiency (PCE) to 5.4% under 1 sun (100 $mWcm^{-2}$) irradiation, in comparison to either Au or Cdot CEs. Moreover, since the preparation process we propose is easy without the requirement of high temperature or expensive equipment, the method shows potential for upscaling.

2. Experimental section

2.1. Synthesis of the Cdots

The Cdots were synthesized by a microwave process reported previously [25]. Citric acid (3 g, Duksan Chemical) was mixed with urea (3 g, Shinyo Chemical) in 10 mL of distilled water by vigorous stirring. The carbonization process was carried out by heating the transparent solution in a domestic microwave oven (700 W) for 4 min. The dark brown solution obtained was cooled down to room temperature and centrifuged at 7000 rpm for 30 min to remove the large black aggregates. The supernatant containing Cdots was neutralized by sodium bicarbonate and washed with deionized (DI) water several times. The black Cdot solid was collected after drying in a vacuum oven.

2.2. Characterization of the Cdots

Atomic force microscopy (AFM) images were acquired in the tapping mode on a MultiMode 8 (Bruker) microscope with samples prepared by dropping the dispersed Cdots in ethanol on a freshly prepared mica substrate. Fluorescence emission analysis was performed using the FL spectrometer LS 55 (PerkinElmer) with an excitation wavelength (λ_{ex}) of 365 nm. Fourier transform infrared (FTIR) spectra were obtained using the FT-IR 4100 spectrophotometer (Jasco, Japan). FT-Raman spectra were acquired using by a FT-Raman spectrometer (Bruker) with a 514 nm laser source.

2.3. Preparation of the working electrodes

The working electrodes were prepared as described previously [15]. Briefly, a 50 nm-thick ZnO buffer film was sputtered onto fluorine-doped tin oxide (FTO) glass (~8 Ω/□, Pilkington, USA), which was then immersed in an aqueous solution containing $Zn(NO_3)_2.6H_2O$ (0.01 M) and NH_4OH (0.5 M) at 95 °C for 12 h. The ZnO nanowire (NW) electrodes were sensitized with CdS using the ion-layer adsorption and reaction. For this, the electrodes were dipped into an aqueous solution of $CdSO_4$ (200 mM) for 30 s, rinsed with deionized water for 30 s, dipped in an aqueous solution of Na_2S (200 mM) for 30 s, and finally rinsed with DI water for 30 s. Then, the CdSe QDs were deposited in situ on the CdS/ZnO NWs by chemical bath deposition from an aqueous solution with $Cd(CH_3COO)_2$ (concentration = 2.5 mM, Cd ion source), Na_2SeSO_3 (concentration = 2.5 mM, Se ion source), and NH_4OH (concentration = 45 mM, complexing agent) at 95 °C for 3 h. The QDs were deposited from a home-built bath equipped with a teflon-bladed electric stirrer and a teflon substrate holder. The bath temperature was adjusted to the desired temperature using a thermostat. To achieve suitable loading of CdSe on the CdS/ZnO-NWs, the procedure was repeated thrice. The experimental details of the fabrication of working electrodes are described elsewhere [15].

2.4. Preparation of the CEs

We prepared three different CEs for comparison. The first one contained a sputtered Au CE with a thickness of 70 nm. The second and third samples were Cdot-coated and Cdot-Au NR-coated CEs fabricated as reported in the previous study [26]. Briefly, the Cdot and Cdot-Au NRs were dispersed in a solution of ethanol:Nafion with a volume ratio of 10:1 by ultrasonication for 1 h. The slurry was coated on an FTO glass substrate by the doctor blade method and subsequently dried at 200 °C for 1 h.

2.5. Assembly of the QDSCs

The QDSCs were assembled as described in the previous study [15]. Briefly, the working electrode and the CE were assembled into a sandwich-type cell, which was sealed with a 60 μm-thick thermobonding polymer (Surlyn, DuPont) at 120 °C for 5 min. A drop of the electrolyte composed of Na_2S (0.5 M), S (2 M), and KCl (0.2 M) in methanol/water (the volume ratio of 7:3) was injected in each hole (0.8 mm) located in behind the working electrode. The two holes were sealed with the Surlyn layer.

2.6. Characterization and measurements

The morphologies of the nanohybrid materials were characterized by high-resolution scanning electron microscopy (HRSEM, TOPCON DS-130C), and transmission electron microscopy (TEM, JEM-2100F, Joel, Japan). The chemical states of the nanohybrids were analyzed by EDS (JEM-2100F, Joel, Japan). The photocurrent density-voltage characteristics of the cells were measured under a simulated air mass 1.5 G solar spectrum. The constant light illumination was adjusted to 100 $mWcm^{-2}$ using a national renewable energy laboratory (NREL)-certified silicon reference cell equipped with a KG-5 filter. An active area of 0.25 cm^2 was accurately defined using a mask placed in front of the cell [15]. The electrochemical impedance spectra (EIS) of the counter electrodes were obtained using the symmetric cell configuration with an Ivium potentiostat. The frequency range was varied from 100 kHz to 100 mHz with a modulation amplitude of 5 mV at a 0 V bias voltage [27]. The EIS spectra were fitted using the Z-view software package.

3. Results and discussion

As mentioned earlier, the Cdots were prepared by a simple microwave synthesis reported previously (details are provided in the Supporting Information) [25]. The Cdots were nanoparticles with heights in the range 1.0–1.5 nm (Fig. S1), exhibiting blue emission (λ_{em} = 440 nm) at λ_{ex} = 365 nm (Fig. S2). FT-IR

spectroscopy indicated that the surface functional groups on the Cdots are carboxylic and primary amine groups (Fig. S3(a)). The FT-Raman spectrum (Fig. S3(b)) exhibited two broad peaks centered at ~1362 cm^{-1} and ~1604 cm^{-1}, which can be assigned to the disorder-induced D band (sp^3 structure) and the first order Raman-allowed G band (sp^2 structure), respectively. Hence, the Cdots consist of both amorphous and crystalline molecular structures. The intensity ratio of D to G band (I_D/I_G) was 0.89, indicating the structural similarity of the Cdots to graphite [25].

These Cdots were used for the preparation of Cdot-Au NRs consisting of a dense array of Au branches. For the synthesis of Cdot-Au NRs, 0.031 g $HAuCl_4$ was added into 20 mL Cdot solution (1 mg Cdot/10 mL H_2O), followed by mixing with 1 mL formic acid at room temperature. The reaction was kept at room temperature for 16 h and at 80 °C for 15 min [28]. The synthesized Cdot-Au NRs were precipitated at the bottom of the flask (Fig. S4). The overall structure of the as-synthesized nanocomposites was characterized by HRSEM and TEM, as shown in Fig. 1(a) and (b), respectively. All the synthesized particles exhibited three dimensional (3D) raspberry-like shapes with an average diameter of ~200 nm. Since the individual particles consisted of a large number of Au branches, the surface of the nanocomposites was very rough. High magnification TEM of a single Cdot-AuNR clearly shows the detailed morphologies of the NRs. All the branches of the NRs were thick spheroidal Au particles (~10 nm in diameter and ~15 nm in length) (Fig. 1(c)). The high-resolution TEM image (Fig. 1(d)) of a single Au branch exhibits its crystalline structure with highly ordered fringes with a lattice spacing of 2.03 Å, which corresponds to the Au{200} interplanar distance (JCPDS 04-0784). Since HRTEM analysis did not clearly show the presence of Cdots in the Au NRs, HAADF-

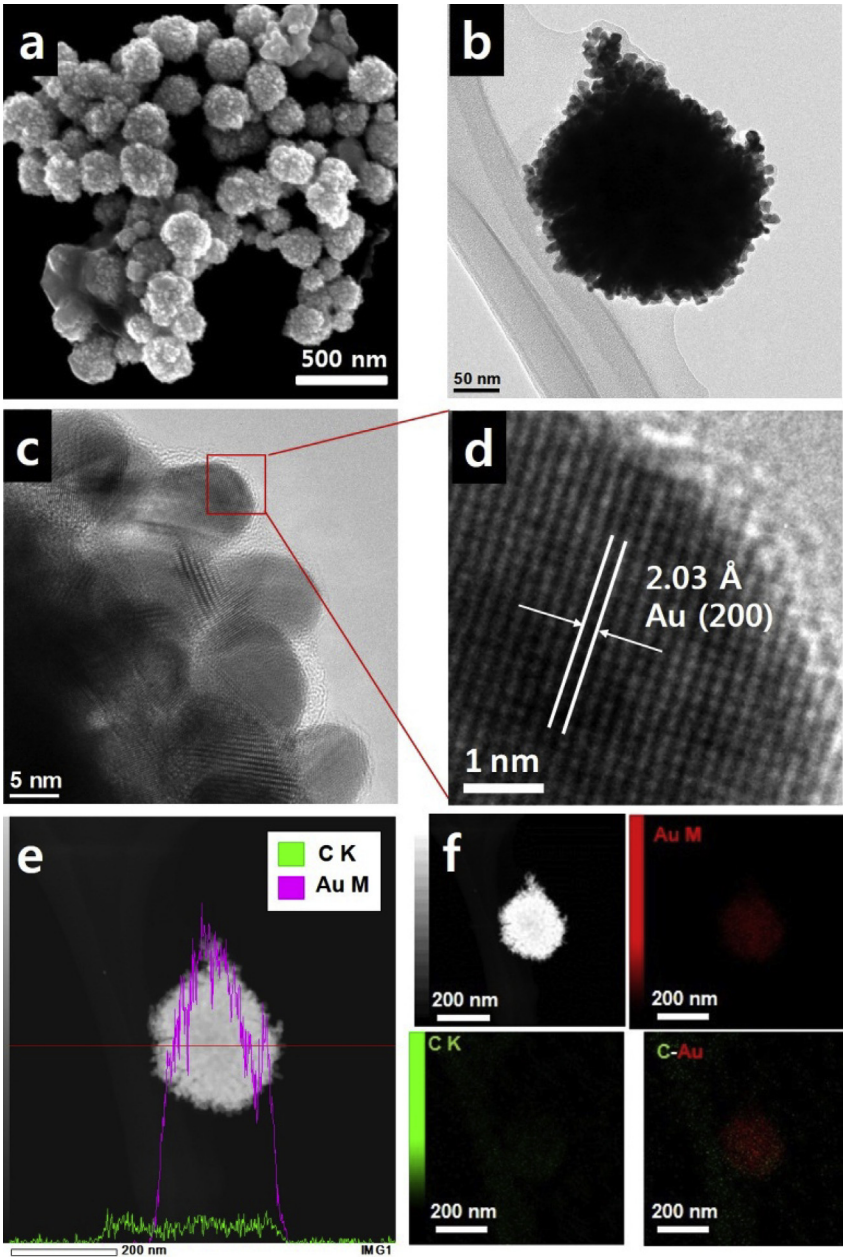

Fig. 1. (a) HRSEM image of Cdot-Au NRs, (b) TEM image of a single Cdot-Au NR, (c) and (d) magnified TEM images, and (e) HAADF-STEM image and cross sectional compositional line profile of a single Cdot-Au NR. The EDX linescan intensities confirm the presence of a Cdot inside the Au fringes. (f) HAADF-STEM-EDS elemental mapping of a Cdot-Au NR. (A colour version of this figure can be viewed online.)

STEM-EDS measurements were carried out to clarify the elemental composition (Table S1–S4). As shown in Fig. 1(e), the EDS cross sectional compositional line profile revealed the presence of the Cdot within the Au fringes of a single nanoraspberry (Fig. S5 and Table S1). The EDS elemental mapping also confirmed the uniform distribution of carbon over the entire raspberry-like structure, overlapping with the Au distribution (Fig. 1(f), Fig. S6 and Table S4). Au is the dominant component in the Cdot-Au NRs. As a control experiment, an identical synthesis procedure was carried out without the Cdots in the Au precursor solution to produce only heterogeneous Au NPs (Fig. S7). This indicates that the observed anisotropic growth of the Au branches can probably be attributed to the presence of Cdots. In the current method, once the Au nuclei are formed and immobilized on the surface of a Cdot after reduction by formic acid, the Au nuclei act as catalytic sites for the further reduction of the Au precursors. Simultaneously, the Cdots adsorb on the Au nuclei due to the existence of various functional groups such as −NH, −OH, −CN, −CO on the Cdot surface. The existence of the functional groups on the Cdot surface has been confirmed by FTIR (Fig. S3). This anisotropic growth of Au on favorable sites along with the deposition of Cdots yields the development of Au branches with the uniform distribution of Cdots across the NR structure [29].

We employed the Cdot-Au NR to fabricate the CE of QDSCs because of its electrochemical properties. Fig. 2(a) shows the schematic diagram of the cell assembly. The working electrode and the CE were assembled into a sandwich type ZnO NW/CdS/CdSe cell (see Supporting Information for details). For comparison, we also prepared CEs using Cdot or Aualone. Fig. 2(b) shows the current density versus voltage (J–V) characteristics obtained with various CEs (the details are summarized in Table 1). The J-V curves for the cells showed that the solar cell performance was considerably influenced by the choice of the CE materials. The J-V curve of the cell employing the Cdot-Au NR CE exhibits an open-circuit voltage (V_{OC}) of 708 mV, a short-circuit current density (J_{SC}) of 16.6 mAcm^{-2}, and a fill factor (FF) of 46%, resulting in an average PCE of 5.4%. In contrast, the QDSC using the Au-sputtered CE exhibits a J_{SC} of 13.2 mAcm^{-2}, a FF of 39%, and a PCE of 3.6%, while Cdot by itself was not a suitable CE material, showing a much lower PCE (0.18%). Furthermore, QDSC employing Au NP-based CE also showed a low PCE of 0.7%. This value is remarkably lower than that of the device assembled by the Cdot-Au NR electrode (5.4%). The high performance of the QDSCs using the Cdot-Au NR-based CE is attributed to its much larger surface area than the Au-sputtered CE, leading to an increase in the number of electrocatalytic active sites.

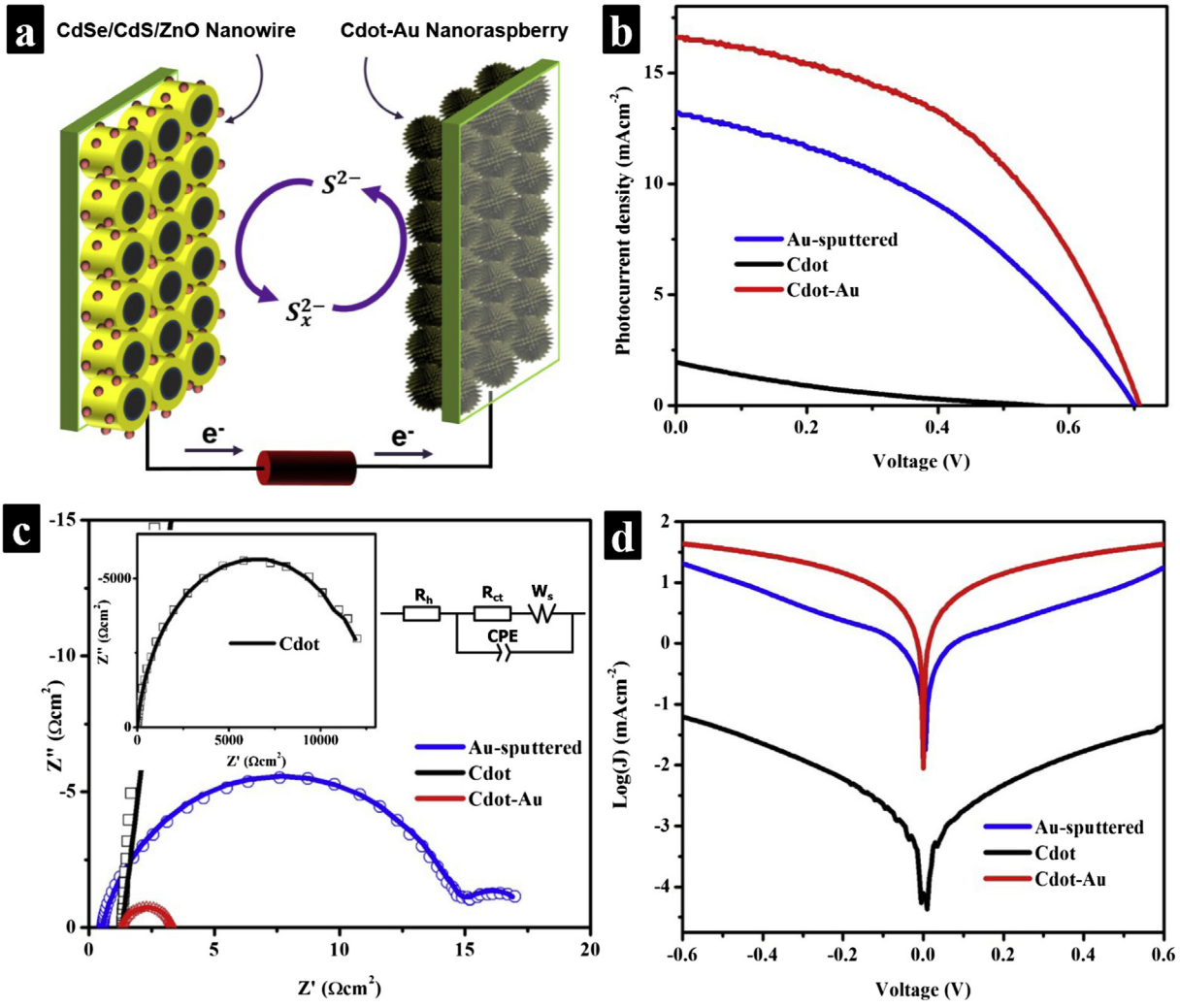

Fig. 2. (a) Schematic of a QDSC with a CdSe/CdS/ZnO-NW photoelectrode and a Cdot-Au NR CE. (b) Characteristic current density-voltage curves of QDSCs measured under standard conditions with different CEs. (c) Nyquist plots of the symmetrical dummy cells with two identical CEs. Inset: Nyquist plot of the symmetrical dummy cell equipped with Cdot CEs (left) and equivalent circuit diagram used to fit the observed impedance spectra (right). (d) Tafel curves of different dummy cells similar to those used for the EIS measurements. (A colour version of this figure can be viewed online.)

Table 1
Photovoltaic properties of the QDSCs with various CEs.

CE	J_{sc} (mAcm^{-2})	V_{oc} (mV)	FF (%)	η (%)
Au-sputtered	13.2	702	39	3.6
Cdot	2.0	550	16	0.18
Cdot-Au NR	16.6	708	46	5.4

In addition, it has been suggested that Cdots provide electrochemical active sites and improve charge transfer rate due to the presence of many active sites on the Cdot surface [22].

The effect of the CE materials on the QDSC performance was evaluated by electrochemical impedance spectroscopy (EIS), which is closely related to their electrical conductivities and electrocatalytic activities towards regenerating the S^2/S_x^{2-} redox couple [15]. Fig. 2(c) shows the Nyquist plots of the symmetric cells fabricated with two identical CEs. The spectra were fitted with an equivalent circuit using the Z-view software, which is presented as the upper right inset in Fig. 2(c). Table 2 lists the fitting parameters. The charge transfer resistance (R_{ct}) of the Cdot-Au NR CE was as small as 2.02 Ωcm^2, while that of the Cdot and Au-sputtered CEs were 12404.81 and 14.12 Ωcm^2, respectively, indicating the superior charge transfer and electrocatalytic ability of the Cdot-Au NR at the CE/electrolyte interface. The lower value of R_{ct} also reflects an increase in the current density ($J_o = RT/nFR_{ct}$, where R is the gas constant, T is the temperature, n is the number of electrons involved in the reduction of the polysulfide electrolyte, and F is Faraday's constant), as shown in Table S5. This observation is consistent with the results obtained from the Tafel zones shown in Fig. 2(d). As shown in Fig. 2(d), the Cdot-Au NR CE exhibits higher limiting diffusion current density (J_{lim}) than the other CEs from the diffusion zone, indicating that Cdot-Au NR CE shows the largest diffusion coefficient (D) compared to other CEs: $D = lJ_{lim}/2n$FC where l and C represent the spacer thickness and the electrolyte concentration, respectively. Moreover, from the Tafel-polarization analysis, Cdot-Au NR CE exhibits the highest electrocatalytic activity in reducing S_n^{2-} to nS^{2-} in comparison to Cdot or Au-sputtered CEs (Fig. 2(d)). The high FF and J_{sc} may be explained on the basis of the high exchange current density (J_o) value [30]. The constant phase element (CPE) data confirmed that the active surface area of the Cdot-Au NR CE is much larger than the values shown by the other CEs (Table S5). A high value of the Warburg diffusion impedance (Z_w) indicates a slow diffusion of the redox couple in the polysulfide electrolyte. The lower value Z_w of the Cdot-Au NR CE compared to that of the Au-sputtered and Cdot electrodes is attributed to the large surface area of the NRs. Further, it is well-known that a decrease in both R_{ct} and Z_w causes a reduction in the total internal resistance, resulting in an increase in the FF and J_{sc} of the QDSC [31]. The series resistance ($R_s = R_h + R_{ct} + Z_w$ (R)) of the cell employing the Cdot-Au NR electrode was 3.34 Ωcm^2, lower than the values exhibited by the equivalent devices employing Au-sputtered (17.52 Ωcm^2) or Cdot (13037.06 Ωcm^2) CEs (Table 2). These results are in good agreement with the PV parameters of the QDSCs. The stability test of the cell using the Cdot-Au NR CE shows no noticeable change in the R_h after three weeks (Fig. S8 and Table S6).

Table 2
The fitted impedance parameters extracted from the EIS spectra of the QDSCs with various CEs.

CE	R_{ct} (Ωcm^2)	Z_w (Ωcm^2)	R_s (Ωcm^2)
Au-sputtered	14.12	2.87	17.52
Cdot	12404.81	630.63	13037.06
Cdot-Au NR	2.02	0.02	3.34

4. Conclusion

We synthesized Cdot-Au NRs consisting of a dense array of Au branches by a simple one-pot chemical reduction of $HAuCl_4$ in a Cdot solution. The resulting material exhibited a high electrocatalytic activity toward the reduction of S_n^{2-} to nS^{2-} and showed potential as a CE for QDSCs. The cell using the Cdot-Au NR CE achieved a high power conversion efficiency of 5.4% with 26% J_{sc} and 18% FF. These features render Cdot-Au NRs as highly promising counter electrode materials for QDSCs. Since the synthesis process is facile and cost-effective for large-scale applications, we believe that this method can be applied to the synthesis of various nanohybrid materials for a wide range of applications.

Acknowledgments

This research was supported by the National Research Foundation (NRF) grant funded by the Korea government (MSIP) (NRF-2014R1A2A2A01006994). This work was also supported by the Korea CCS R&D Center (KCRC) grant funded by the Korea government (MSIP) (2014M1A8A1049345), by the NRF-RFBR Joint Research Program through the National Research Foundation (NRF-2013K2A1A7076282), by the National Research Foundation Postdoctoral Fellowship Program 2014 (NRF-2014K2A4A1034681) and by the Korea Brain Pool Program 2013 (131S-6-3-0538). P. K., R. R., and S. K. acknowledge support from the Institute for Basic Science under grant number IBS-R004-D1.

Appendix A. Supplementary data

Supplementary data related to this article can be found at http://dx.doi.org/10.1016/j.carbon.2015.09.023.

References

[1] J.G. Radich, R. Dwyer, P.V. Kamat, Cu_2S reduced graphene oxide composite for high-efficiency quantum dot solar cells. Overcoming the redox limitations of S_2^-/S_n^{2-} at the counter electrode, J. Phys. Chem. Lett. 2 (2011) 2453.
[2] M.C. Hanna, A.J.J. Nozic, Solar conversion efficiency of photovoltaic and photoelectrolysis cells with carrier multiplication absorbers, J. Appl. Phys. 100 (2006) 074510.
[3] P.V. Kamat, Boosting the efficiency of quantum dot sensitized solar cells through modulation of interfacial charge transfer, Acc. Chem. Res. 45 (2012) 1906.
[4] P. Maraghechi, A.J. Labelle, A.R. Kirmani, X. Lan, M.M. Adachi, S.M. Thon, et al., The donor-supply electrode enhances performance in colloidal quantum dot solar cells, ACS Nano 7 (2013) 6111.
[5] Y. Lang, Y.S. Lo, Highly efficiency quantum-dot-sensitized solar cell based on co-sensitization of CdS/CdSe, Adv. Funct. Mater. 19 (2009) 604.
[6] Y. Bai, C. Han, X. Chen, H. Yu, X. Zong, Z. Li, et al., Boosting the efficiency of quantum dot sensitized solar cells up to 7.11% through simultaneous engineering of photocathode and photoanode, Nano Energy 13 (2015) 609.
[7] V. Chakrapani, D. Baker, P.V. Kamat, Understanding the role of the sulfide redox couple (S^{2-}/S_n^{2-}) in quantum dot-sensitized solar cells, J. Am. Chem. Soc. 133 (2011) 9607.
[8] D.H. Youn, M. Seol, J.Y. Kim, J.W. Jang, Y. Choi, K. Yong, J.S. Lee, TiN nanoparticles on CNT–graphene hybrid support as noble-metal-free counter electrode for quantum-dot-sensitized solar cells, ChemSusChem 6 (2013) 261.
[9] V.D. Dao, W. Choi, K. Yong, L.L. Larina, O. Shevaleevskiy, H.S. Choi, A facile synthesis of bimetallic AuPt nanoparticles as a new transparent counter electrode for quantum-dot-sensitized solar cells, J. Power Sources 274 (2015) 831.
[10] Z. Yang, C.Y. Chen, C.W. Liu, C.L. Li, H.T. Chang, Quantum dot–sensitized solar cells featuring CuS/CoS electrodes provide 4.1% efficiency, Adv. Energy Mater. 1 (2011) 259.
[11] Z. Yang, C.Y. Chen, C.W. Liu, C.L. Li, H.T. Chang, Electrocatalytic sulfur electrodes for CdS/CdSe quantum dot-sensitized solar cells, Chem. Commun. 46 (2010) 5485.
[12] J.W. Lee, D.Y. Son, T.K. Ahn, H.W. Shin, I.Y. Kim, S.J. Hwang, et al., Quantum-dot-sensitized solar cell with unprecedentedly high photocurrent, Sci. Rep. 3 (2013) 1.
[13] S.T. Finn, J.E. Macdonald, Petaled molybdenum disulfide surfaces: facile synthesis of a superior cathode for QDSSCs, Adv. Energy Mater. 4 (2014) 1400495.
[14] D.M. Li, L.Y. Cheng, Y.D. Zhang, Q.X. Zhang, X.M. Huang, Y.H. Luo, et al.,

Development of Cu_2S/carbon composite electrode for CdS/CdSe quantum dot sensitized solar cell modules, Sol. Energy Mater. Sol. Cells 120 (2014) 454.
[15] M. Seol, H. Kim, Y. Tak, K. Yong, Novel nanowire array based highly efficient quantum dot sensitized solar cell, Chem. Commun. 46 (2010) 5521.
[16] M. Ye, C. Chen, N. Zhang, X. Wen, W. Guo, C. Lin, Quantum-dot-sensitized solar cell employing hierarchical Cu_2S microsphere wrapped by reduced graphene oxide nanosheets as effective counter electrodes, Adv. Energy Mater. 4 (2014) 1301564.
[17] V.D. Dao, Y. Choi, K. Yong, L. Larina, H.S. Choi, Graphene-based nanohybrid materials as the counter electrode for highly efficient quantum-dot-sensitized solar cells, Carbon 84 (2015) 383.
[18] M. Soel, D.H. Youn, J.Y. Kim, J.W. Jang, M. Choi, J.S. Lee, et al., Mo-compound/CNT-graphene composites as efficient catalytic electrodes for quantum-dot-sensitized solar cells, Adv. Energy Mater. 4 (2013) 1300775.
[19] L. Chen, J. Jin, X. Shu, J. Xia, Solid state synthesis of poly(3,4-ethylenedioxythiophene) as counter electrode for dye-sensitized solar cell, J. Power Sources 248 (2014) 1234.
[20] M.H. Yeh, C.P. Lee, C.Y. Chou, L.Y. Lin, H.Y. Wei, C.W. Chu, et al., Conducting polymer-based counter electrode for a quantum-dot-sensitized solar cell (QDSSC) with a polysulfide electrolyte, Electrochim. Acta 57 (2011) 277.
[21] L. Kavan, J.H. Yum, M.K. Nazeeruddin, M. Gratzel, Graphene nanoplatelet cathode for Co(III)/(II) mediated dye-sensitized solar cells, ACS Nano 11 (2011) 9171.
[22] L. Chen, C.X. Guo, Q. Zhang, Y. Lei, J. Xie, S. Ee, et al., Graphene quantum-dot-doped polypyrrole counter electrode for high-performance dye-sensitized solar cells, ACS Appl. Mater. Inter. 5 (2013) 2047.
[23] C.C. Wang, S.Y. Lu, Carbon black-derived graphene quantum dots composited with carbon aerogel as a highly efficient and stable reduction catalyst for the iodide/tri-iodide couple, Nanoscale 7 (2015) 1209.
[24] W. Chen, M. Wang, T. Qian, H. Cao, S. Huang, Q. He, et al., Rational design and fabrication of skeletal Cu_7S_4 nanocages for efficient counter electrode in quantum dot-sensitized solar cell, Nano Energy 12 (2015) 186.
[25] S. Qu, X. Wang, Q. Lu, X. Liu, L. Wang, A biocompatible fluorescent ink based on water-soluble luminescent carbon nanodots, Angew. Chem. Int. Ed. 51 (2012) 12215.
[26] A. Kaniyoor, S. Ramaprabhu, Gold nanoparticle decorated multi-walled carbon nanotubes as counter electrode for dye sensitized solar cells, J. Nanosci. Nanotech. 12 (2012) 8323.
[27] V.D. Dao, C.Q. Tran, S.H. Ko, H.S. Choi, Dry plasma reduction to synthesize supported platinum nanoparticles for flexible dye-sensitized solar cells, J. Mater Chem. A 1 (2013) 4436.
[28] S. Sun, D. Yang, D. Villers, G. Zhang, E. Sacher, J.P. Dodelet, Template- and surfactant- free room temperature synthesis of self-assembled 3D Pt nano-flowers from single-crystal nanowires, Adv. Mater. 20 (2008) 571.
[29] S. Sun, D. Yang, G. Zhang, E. Sacher, J.P. Dodelet, Synthesis and characterization of platinum nanowire-carbon nanotube heterostructures, Chem. Mater. 19 (2007) 6376.
[30] S.I. Cha, B.K. Koo, S.H. Seo, D.Y. Lee, Pt-free transparent counter electrodes for dye-sensitized solar cells prepared from carbon nanotube micro-balls, J. Mater Chem. 20 (2010) 659.
[31] L. Han, N. Koide, Y. Chiba, A. Islam, R. Komiya, N. Fuke, et al., Improvement of efficiency of dye-sensitized solar cells by reduction of internal resistance, Appl. Phys. Lett. 86 (2005) 213501.